Plasma Science and Technology

PAPER

Bench test of interferometer measurement for the Keda Reconnection eXperiment device (KRX)

To cite this article: Dongkuan LIU *et al* 2022 *Plasma Sci. Technol.* **24** 064005

View the article online for updates and enhancements.

You may also like

- Design of interferometer system on Versatile Experiment Spherical Torus (VEST) at Seoul National University
  D H Choi, Y H An, K J Chung et al.
- Measurement of the gold–gold bond rupture force at 4 K in a single-atom chain using photon-momentum-based force calibration
  D T Smith and J R Pratt
- Development and preliminary experimental results of a high-temporal-resolution terahertz solid-source interferometer on EAST
  J. Li, S.X. Wang, H.Q. Liu et al.

This content was downloaded from IP address 202.38.84.17 on 08/07/2022 at 00:36

© 2022 Hefei Institutes of Physical Science, Chinese Academy of Sciences and IOP Publishing Printed in China and the UK Plasma Science and Technology

Plasma Sci. Technol. **24** (2022) 064005 (6pp) https://doi.org/10.1088/2058-6272/ac5789

Bench test of interferometer measurement for the Keda Reconnection eXperiment device (KRX)

Dongkuan LIU (刘东宽)[1], **Weixing DING** (丁卫星)[1,2,*], **Wenzhe MAO** (毛文哲)[2], **Qiaofeng ZHANG** (张乔枫)[1], **Longlong SANG** (桑龙龙)[1], **Quanming LU** (陆全明)[1] and **Jinlin XIE** (谢锦林)[1,2]

[1] CAS Key Lab of Geoscience Environment, School of Earth and Space Sciences, University of Science and Technology of China, Hefei 230026, People's Republic of China
[2] Department of Plasma Physics and Nuclear Engineering, University of Science and Technology of China, Hefei 230026, People's Republic of China

E-mail: wxding@ustc.edu.cn

Received 22 November 2021, revised 21 January 2022
Accepted for publication 22 February 2022
Published 26 May 2022

Abstract

Motivated by the need of the electron density measurement for the Keda Reconnection eXperiment (KRX) facility which is under development, an interferometer system has been designed and tested in bench. The 320 GHz solid-state microwave source with 1 mm wavelength is used to fulfill the high phase difference measurement in such low temperature plasma device. The results of the bench test show that the phase difference is accurately measured. In contrast to tens of degrees of phase shift expected to be measured on the KRX, the system noise ($\sim 1^{\circ}$) is low enough for the KRX diagnostics. In order to optimize the system for better performance, we utilize the Terasense sub-THz imaging system to adjust alignment. The interferometer system has also been calibrated via changing of the optical path length controlled by the piezo inertial motor. Simultaneously, high density polyethylene thin film is introduced successfully to change a tiny phase difference and test the sensitivity of the interferometer system.

Keywords: magnetic reconnection, diagnostics, interferometer

(Some figures may appear in colour only in the online journal)

1. Introduction

Magnetic reconnection, known as an important physical process, can abruptly convert the stored magnetic energy to particle energy, and is associated with amounts of explosive phenomena in interplanetary space, solar atmosphere, the earth's magnetosphere, and laboratory experiments [1–10]. Understanding the magnetic reconnection mechanism and structure remains a key scientific challenge. Compared with *in situ* observation and theoretical numerical simulation, the ground experiment in the laboratory has a large amount of advantages in studying magnetic reconnection: (I) controlled conditions, (II) numerous-point measurements, (III) reproducibility, and (IV) authenticity.

The Keda Reconnection eXperiment device (KRX) has been built for investigating the fundamental reconnection physics. The KRX is a ϕ 3 $\times$ 10 m cylindrical vacuum chamber facility, as shown in figure 1. The plasma is produced by hot cathode source in the top of the vacuum chamber [11]. The electrons emitted from the hot cathode ionize the inert gas (argon or helium) and the uniform plasma can be produced. The axial magnetic field is produced by 10 coils with a maximum value of magnetic field B = 100 Gauss. The current flows through a pair of drive plates to create the opposed magnetic field, resulting in anti-parallel reconnection. The reconnection magnetic field can be controlled in 0–500 Gauss. The experiment size is 2.5 $\times$ 1 m^2, the plasma density

* Author to whom any correspondence should be addressed.

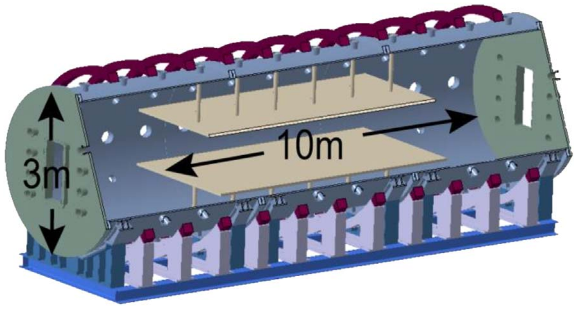

Figure 1. The machine drawing of the KRX device.

(10^{16}–$10^{19}\ \mathrm{m}^{-3}$) and the electron/ion inertial length ($c/\omega_{pe}(\omega_{pi})$) can be controlled via discharge by different inert gases. The overall experimental size is 5–10 times ion inertial lengths which satisfies the electron scale and ion scale reconnection investigation. The facility is housed in the east of Hefei and the first discharge has been completed in 2021. The KRX is expected to start to run formally in 2022. Meanwhile, the plasma diagnostics is also on the way.

The main diagnostics methods in reconnection experiments are based on the probe measurement (magnetic probes, Rogowski coils, Langmuir probes and speed probes, etc), like the experiments in MRX [4, 12], LAPD [13, 14] and TREX [15]. Nevertheless, the probe diagnostic is difficult to measure the absolute density. In addition, the thin current sheet measurement remains a challenge in laboratory plasma due to disturbance of matter probes. The polarimeter-interferometer diagnostic, known as no perturbation electron/current density and magnetic field measurement means, has been used for plenty of fusion tokamak facilities [16–19], and it also contributes to the feedback control of plasma density. Motivated by the demand of advanced electron density and current measurement for the low temperature plasma, it is necessary for us to develop polarimeter-interferometer diagnostics technology for the KRX facility.

In this paper, section 2 gives the schematic of the polarimeter-interferometer system for the KRX, section 3 presents the bench test of the interferometer system, the overall summary and the future plan are given in section 4.

2. The layout of conception design of the KRX interferometer system

As shown in figure 2(a), the KRX has 6 pairs of rectangular windows and dozens of circular windows in the cross section, and each window is allowed for the probes, microwave and optical diagnostics. The size of the rectangular window is $100 \times 25\ \mathrm{cm}^2$ and the radius of the circular window is 12.5 cm. The conception design of the polarimeter-interferometer measurement for the KRX has been finished. As shown in figures 2(b) and (c), the design applies the heterodyne Mach-Zehnder type polarimetry-interferometer detection method [20]. The probing beam passes through the plasma via two long flanged windows horizontally, the long-flanged windows are sealed with high density polyethylene (HDPE) so that the microwave can pass through. The

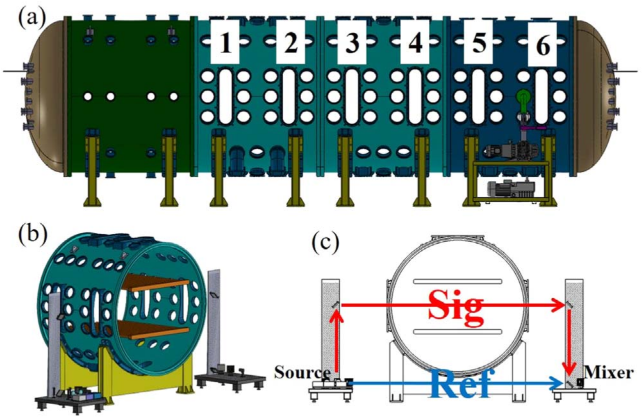

Figure 2. (a) The machine structure of the KRX device. The main diagnostics windows are 6 pairs of rectangular windows and dozens of circular ports in the middle of the vacuum chamber. (b) The conception design of the polarimeter-interferometer diagnostics system for KRX. (c) The optical path design of the interferometer system. The heterodyne detection method is utilized in this design, the signal beam passes through the fourth rectangular window, the reference beam bypasses the vacuum chamber, and the two beams are mixed into detectors on the other side. The system will be upgraded to multi-channels eventually.

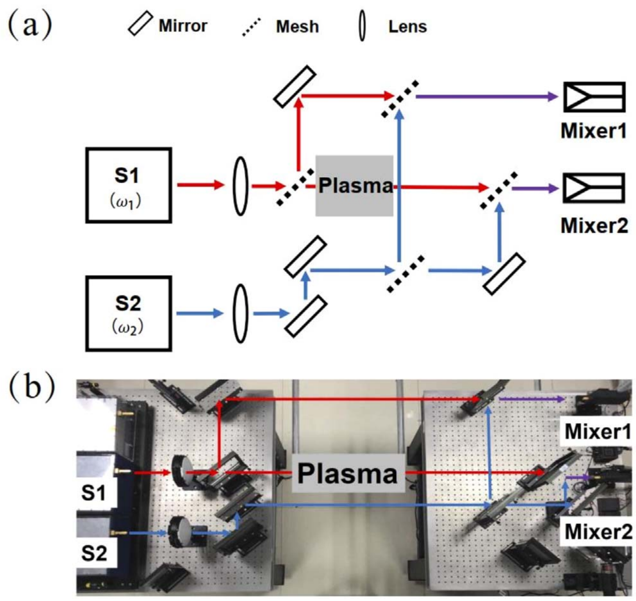

Figure 3. (a) The schematic bench test of the interferometer system and (b) the layout of the optical components on two optical tables. Probing beam is shown as the red, and the reference beam is in blue.

diameter of the beam will be smaller than the width of the rectangular window. The reference beam bypasses the vacuum chamber along the gap of the base, the two beams are combined into the mixer to form heterodyne measurement. The line-integrated density can be measured by the phase difference from the interferometer, which is shown

$$\varphi = 2.82 \times 10^{-15}\lambda \int n_e \mathrm{d}l, \tag{1}$$

where n_e is the electron density, λ is the detection wave wavelength, and l is the path length of plasma. The

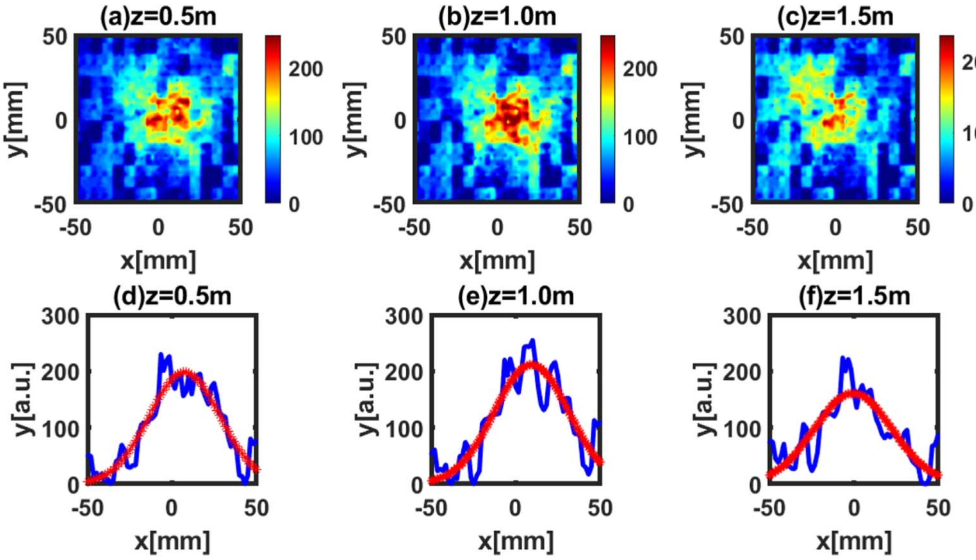

Figure 4. (a)–(c) The relative power distribution of the probe beam along the propagation direction measured by the Terasense sub-THz camera at $z = 0.5$, 1, and 1.5 m, respectively, where z is the distance between the source antenna horn to the camera. (d)–(f) The cuts of the relative power (blue line) of corresponding (a)–(c) along the line $y = 0$ mm, and the red dotted lines represent the Gaussian fitting of the beam relative power.

corresponding magnetic field and current density measurement from the Faraday effect can be expressed as

$$\theta_{\mathrm{f}} = 2.62 \times 10^{-13}\lambda^2 \int n_{\mathrm{e}} B_{||} \mathrm{d}l, \tag{2}$$

where θ_{f} is the measured Faraday rotation angle, $B_{||}$ is magnetic field parallel to the direction of detection wave. The polarimeter-interferometer system will be installed on the fourth rectangular window in 2022, and this optical path can be extended into multiple channels from the middle of the two current plates. Therefore, we can get the electron density and current density profile with the evolution of the reconnection and acquire further understanding of the reconnection physics.

The polarimeter-interferometer diagnostic requires fast time-resolution for magnetic reconnection experiments. The difficulty in the diagnostics is the phase difference measurement in such low density plasma. For this purpose, the proper wavelength ($\sim$1 mm) is selected to ensure there is large enough phase difference to measure [21]. The interferometer phase difference evaluated by the working gases is from $\sim\pi/6$ to 2π which is easily measurable, and thus the density can be accurately determined. Previously, the 650–700 GHz microwaves have been widely and successfully applied in plenty of fusion devices and provide the accurate measurement [16, 18, 22–24]. Nevertheless, for the 320 GHz solid-state sources, the bench test is indispensable to verify measurement feasibility on the KRX.

3. Bench test of the interferometer system

The purpose of the bench test is to optimize and verify the feasibility of the system. The noise of the system largely depends on the optical design and alignment the two beams.

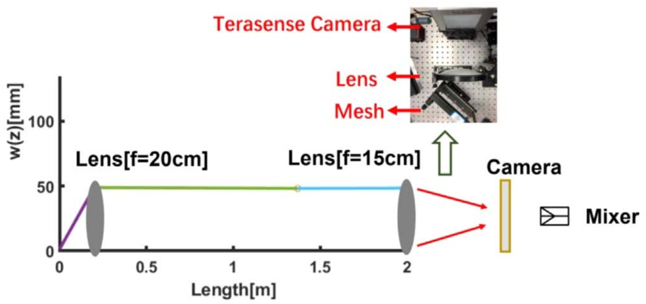

Figure 5. Schematic propagation of the Gaussian beam of the microwave source and the layout of the Terasense camera.

Due to this motivation, the sub-THz camera, movable mirror and the HDPE films are introduced to optimize the design and examine the measurement vability.

3.1. Optical path design of the interferometer system

As shown in figure 3(a), the bench test applies the heterodyne interferometer means [25]. Figure 3(b) presents the layout of the optical components on the two $1 \times 0.8 \times 0.8$ m^3 stages with broadband damping for vibration isolation. Two frequency adjustable 320 GHz (316–324 GHz) solid-state Virginia Diodes Inc (VDI) microwave sources S1(ω_1) and S2(ω_2) are used as the signal sources. The output frequency of the sources can be set with a resolution better than 20 Hz with 15 mW output power. The intermediate frequency (IF) is set to be $\sim$1 MHz (we set the S1 (ω_1) frequency to 320 GHz, and the S2(ω_2) to 320 GHz + IF). The VDI Schottky planar-diode mixers with high response ($\sim$1300 V W^{-1}) are introduced as the detectors [26]. We use the 70 LPI (lines per inch) wire mesh as the beam splitter which is suitable for the budget

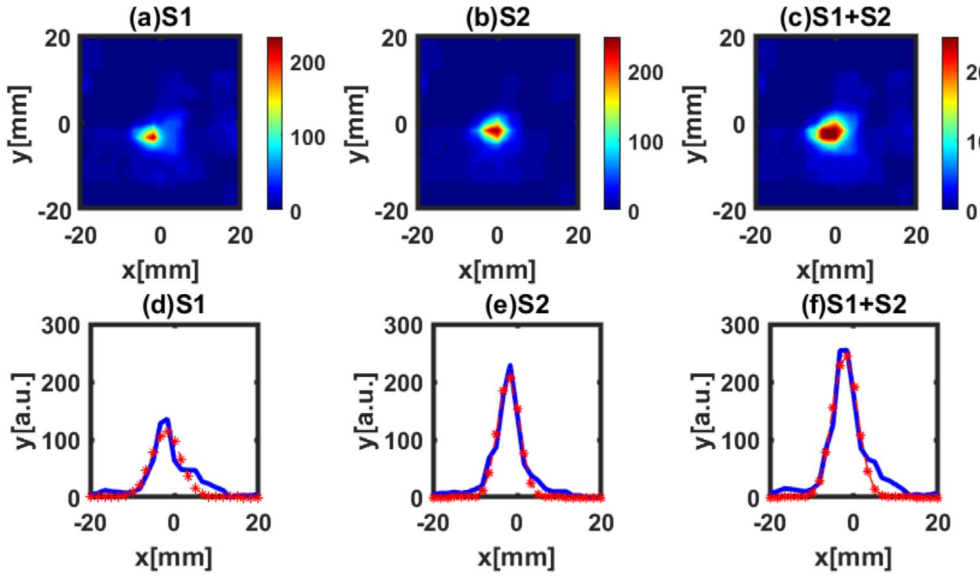

Figure 6. The relative power distributions of microwave beam measured by the sub-THz camera in front of the mixer with the camera placed at the same distance as the focal length of lens (15 cm). (a)–(c) The relative power distributions of microwave sources S1, S2, and the mixing of S1 and S2, respectively. (d)–(f) The cuts of the relative power of corresponding (a)–(c) along the line $y = -1.65$ mm (blue line), the red dotted lines represent the Gaussian fitting of the beam relative power.

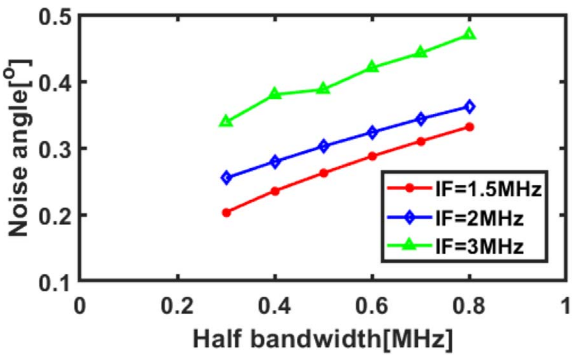

Figure 7. Band-pass filter half bandwidth versus rms phase difference noise for the cases with IF = 1.5, 2 and 3 MHz, respectively. The sampling is 10 MS s^{-1}.

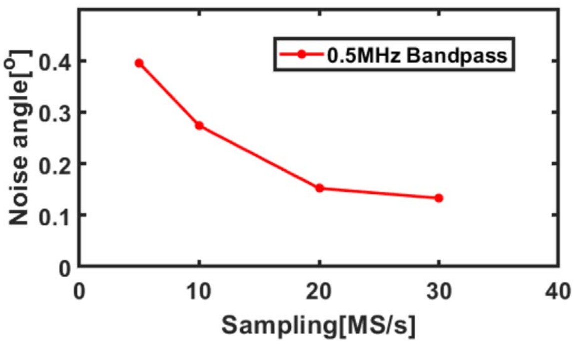

Figure 8. The sampling versus system noise with 0.5 MHz bandpass of 1 MHz IF.

of the 320 GHz microwave (∼50% reflection/transmission). The LABVIEW controlled NI (National Instruments) card with 0–60 MS s^{-1} sampling is utilized as our data acquisition.

All of the optical components are mounted on the optical tables. The optical height is 15.6 cm, and the corresponding meshes and the mirrors are also designed as the same height. The entire optical path is ∼2 m for the signal (reference) chord. The lens (focal length = 20 cm) in front of the microwave source is applied to focusing beams. An additional electromagnetic wave absorbing material (BPUFA-50CV) is added around the mirrors and the meshes to minimize the stray light.

3.2. Alignment of the interferometer system

The beam coming from the antenna horn of the sources propagates in Gaussian profile. The radius of the Gaussian beam is approximately 4.8 cm simulated by ZEMAX (an optical design software) after passing through the focal lens. Despite the two beams are firstly aligned by He-Ne lasers, it is not clear how collinear they are. In other words, it is difficult to determine the profile and the location of the propagation because the placement of the sources and the optical components (meshes, mirrors, etc) still cause deviations. It is necessary to measure the power distribution of the Gaussian beam and evaluate the alignment of the interferometer system.

The Terasense sub-THz camera system (model T15/32/32) is used to image the beams. The camera is sensitive to polarization of incoming power with bandwidth approximately 50–700 GHz. The relative power distributions in figure 4 prove that the probing beam has a Gaussian distribution. The lines fitting show that the waist of the probing beam (∼4 cm) is approximately consistent with the result from the simulation of ZEMAX. The error is most likely that we assume the Gaussian beam propagates from the antenna

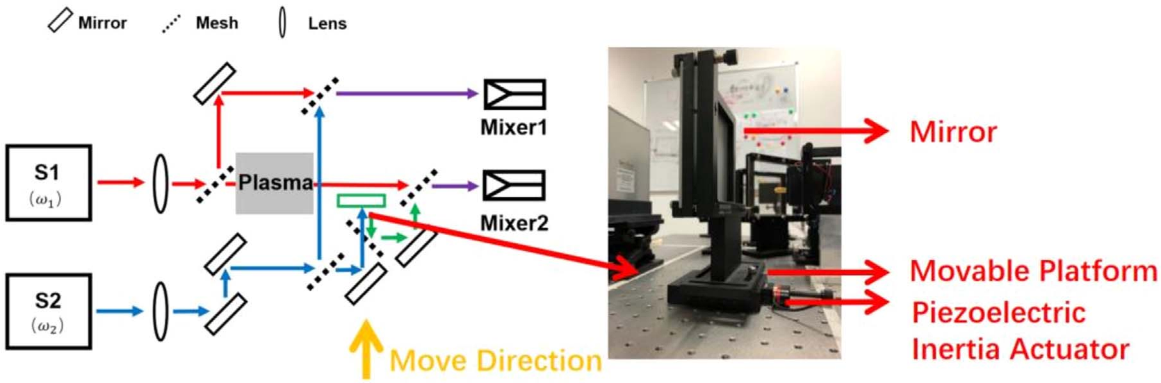

Figure 9. Schematic optical design of the interferometer calibration. A mirror (green) which is perpendicular to the optical path is utilized to adjust optical path difference in the interferometer system. The mirror is mounted on the movable platform which is driven by the piezoelectric inertial actuator. The yellow arrow represents the move direction.

horn, practically, the starting position of the probing beam in the antenna is unknown.

If the collinearity is not well satisfied in front of the mixer, the two beams will introduce the system errors. In order to check the alignment of the two beams, as shown in figure 5, the camera is placed in front of the mixer and a focal lens (focal length = 15 cm) is housed near the camera to increase the intensity of imaging. Figure 6 presents the imaging of the relative power distributions of S1 beam, S2 beam and the mixing of the S1 and S2 in front of the mixer respectively. It can be concluded that the two beams are well overlapped. This indicates that the alignment of the two beams is successfully achieved which is important to optimize the interferometer system.

3.3. Noise and the error analysis

Since frequency difference of the two sources commanded by the computer corresponds to the frequency of IF, the IF signal is clean enough and fully controlled. As shown in [21], the IF in 1 MHz with 10 MS s^{-1} sampling is stable and the root-mean-square (rms) phase difference noise level is low. The stability is the key issue to minimize the phase noise. Nevertheless, the phase noise of the IF largely depends on the stray light, optical deviation and the mixer sensitivity, etc. In addition, the frequency of the IF is also important for the noise evaluation. Figure 7 gives the digital band-pass filter half bandwidth versus rms phase difference noise for the cases with different IFs. The noise increases with a larger IF, but the noise is restricted in the level of $\sim 1^\circ$ with different IFs. This suggests that the minimum line-averaged electron density is $n_e \approx 10^{15}\ m^{-3}$.

Since the phase difference of the interferometer measurement assessment on the KRX is tens of degrees [21], the interferometer system resolution is sufficient to investigate the accurate density measurement. However, the small noise is essential demand for the investigation of the plasma fluctuation and transport [17]. The sampling versus noise in the figure 8 implies that we can also reduce the noise by increasing the sampling because the noise level is effectively improved with the increase of the sampling from 5 MS s^{-1} to 20 MS s^{-1}. However, the noise reduces slowly with higher sampling. Given the above results, the sampling should be reasonably considered. Furthermore, other factors that affect the noise should also be investigated which is significant for the further optimization of the noise.

3.4. Interferometer calibration

In order to calibrate the interferometer system on bench, a piezoelectric inertial actuator with typical step size of 20 nm has been utilized to change optical path length (phase change). As shown in figure 9, a movable mirror (green) is introduced in the optical design to change the optical path. The piezoelectric inertial actuator drives the movable stage to move the mirror, and the move direction follows the direction of the beam as the yellow arrow points to in figure 9. Since the mirror is located far away from the microwave source, the output power reflected back to the source is small and will not damage the microwave source.

The piezo inertial motor controller is used to control the movement of the mirror for continuous jogging. Due to the reflection of the beam, theoretically, the phase difference of the two IFs caused by the jogging of the mirror can be presented as

$$\Delta\varphi(\text{rad}) = 2\pi\frac{\Delta L \times 2}{\lambda}, \tag{3}$$

where ΔL is the jogging distance, λ is the wavelength. Figure 10 gives the calibration results of the interferometer system. After ensemble average, the measured results are pretty well close to the theoretical values which are based on the ideal wave phase theory. The errors in the interferometer system are most likely caused by the installation and optical components deviations.

Because the KRX device is being optimized, the HDPE thin film is used to simulate as the uniform plasma. The key issue of measuring plasma is refractive index measurement. The HDPE thin film is placed in signal beam path as an additional optical offset, as shown the grey 'plasma' area in figure 3(a). The phase difference of the reference chord and

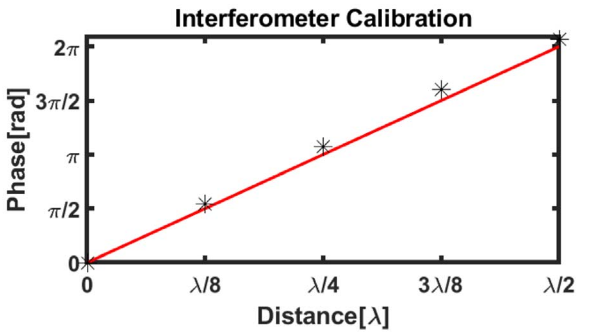

Figure 10. The interferometer calibration. The move distance of the mirror and the measured phase difference, with the red line being the theoretical value and the dots being the measured values.

the signal chord caused by the optical path difference of thin film can be expressed as

$$\Delta\varphi(\mathrm{rad}) = \frac{2\pi(N-1)d}{\lambda}, \tag{4}$$

where N is the refractive index of the thin film, d is the thin film width, and λ is the beam wavelength. Here, we assume the air refractive index is 1, and the refractive index of the thin film can be expressed as

$$N = \frac{\Delta\varphi\lambda}{2\pi d} + 1. \tag{5}$$

Benefiting from optimization of the system, the refractive index measured is 1.60 (the theoretical value is 1.52), which suggests that the measurement error of our interferometer system is negligible.

4. Conclusion

In conclusion, the 320 GHz (1 mm wavelength) probing beam is selected to ensure the sensitivity of the interferometer measurement for KRX facility. The bench tests of solid-state microwave sources show that the IF is stable, and the phase noise ($<1°$) of the system is low enough for electron density diagnostics on the KRX. Besides, to optimize the system, the Terasense sub-THz imaging camera has been introduced to check the propagation of the Gaussian beam and has successfully improved the optical alignment. The interferometer system has been well calibrated by changing the optical path length with the help of precision movement of piezo motor with minimum 20 nm step. The HDPE thin film experiment has also verified that the system is capable of the MHD and turbulence fluctuation measurement. Meanwhile, benefiting from the interferometer system, the development of polarimeter diagnostics system based on Faraday effect for the magnetic field and current measurement will be achieved in the near future.

Acknowledgments

This work is supported by National Natural Science Foundation of China (No. 11975231).

References

[1] Giovanelli R G 1946 *Nature* **158** 81
[2] Forbes T G and Priest E R 1982 *Planet. Space Sci.* **30** 1183
[3] Schindler K 1991 *Geophys. Astrophys. Fluid Dyn.* **62** 37
[4] Ji H T *et al* 1998 *Phys. Rev. Lett.* **80** 3256
[5] Yamada M 1999 *J. Geophys. Res.* **104** 14529
[6] Ding W X *et al* 2004 *Phys. Rev. Lett.* **93** 045002
[7] Angelopoulos V *et al* 2008 *Science* **321** 931
[8] Birn J and Hesse M 2009 *Ann. Geophys.* **27** 1067
[9] Pu Z Y *et al* 2010 *J. Geophys. Res.* **115** A02212
[10] Ding W X *et al* 2006 *Phys. Plasmas* **13** 112306
[11] Hu G H *et al* 2016 *Plasma Sci. Technol.* **18** 918
[12] Ren Y *et al* 2005 *Phys. Rev. Lett.* **95** 055003
[13] Gekelman W *et al* 2020 *J. Plasma Phys.* **86** 925860301
[14] Schroeder J W R *et al* 2021 *Nat. Commun.* **12** 3103
[15] Olson J *et al* 2016 *Phys. Rev. Lett.* **116** 255001
[16] Ding W X *et al* 2010 *Rev. Sci. Instrum.* **81** 10D508
[17] Ding W X *et al* 2003 *Phys. Rev. Lett.* **90** 035002
[18] Chen J *et al* 2018 *Rev. Sci. Instrum.* **89** 10B101
[19] Ding W X *et al* 2018 *Rev. Sci. Instrum.* **89** 10B103
[20] Brower D L *et al* 2001 *Rev. Sci. Instrum.* **72** 1077
[21] Liu D K *et al* 2021 *Rev. Sci. Instrum.* **92** 053516
[22] Xie J L *et al* 2014 *Rev. Sci. Instrum.* **85** 11D828
[23] Mao W Z *et al* 2021 *Rev. Sci. Instrum.* **92** 053514
[24] Liu H Q *et al* 2014 *Rev. Sci. Instrum.* **85** 11D405
[25] Dodel G and Kunz W 1978 *Infrared Phys.* **18** 773
[26] Ding W X *et al* 2014 *Rev. Sci. Instrum.* **85** 11D406